Dynamic Geometrical Calibration for 3-D Cerebral Angiography

N. Navab A. Bani-Hashemi M. Mitschke
Siemens Corporate Research
755 College Road East
Princeton, NJ 08540, USA

D.W. Holdsworth R. Fahrig
Imaging Research Laboratories
University of Western Ontario
London Ontario, N6A 5C1, Canada

A.J. Fox
University Hospital, 339 Windermere Rd.
London Ontario, N6A 5A5, Canada

R. Graumann
Siemens AG, Medical Engineering
Erlangen, Germany, D-91050

ABSTRACT

Recently there has been increasing interest in obtaining three-dimensional reconstructions of arterial vessels from multiple planar radiographs (obtained at angles around the object). Interventional angiography is the motivating application behind this research. Different methods have been proposed to acquire the planar data such as a gantry mounted x-ray image intensifier (XRII) or a C-arm mounted XRII. In order to obtain a three-dimensional reconstruction from a C-arm mounted XRII the trajectory of the source and detector system must be characterized.

We have designed a calibration system that provides the necessary trajectory information using uniquely identifiable markers positioned on a cylinder. This calibration ring is to be placed around the patient's head, and consists of steel balls positioned in a predefined arrangement on a cylindrical acrylic support. The balls are arranged such that calibration can be done from almost any partial view, allowing reconstruction of a region of interest (ROI). Steel balls are placed around an acrylic cylinder, restricted to a band approximately 8.5 mm wide, thereby obscuring only a small fraction of the image. In this case the radiograph includes the region of interest (ROI) as well as a partial view of the calibration ring. This enables us to recover the geometry of X-ray imaging system from each individual frame. We call this process "dynamic calibration" as opposed to "off-line" calibration procedures which try to characterize the motion of C-arm before introducing the patient.

Keywords: Geometrical Calibration, 3-D Cerebral Angiography, C-arm Geometry, Pose Determination, Marker Detection, 3-D/2-D Matching, Reconstruction of ROI.

1 INTRODUCTION

Recently there has been increasing interest in obtaining three-dimensional reconstructions of arterial vessels from multiple planar radiographs (obtained at angles around the object). Interventional angiography is the motivating application behind this research. Different methods have been proposed to acquire the planar data such as a gantry mounted x-ray image intensifier (XRII) or a C-arm mounted XRII. In order to obtain a three-dimensional reconstruction from a C-arm mounted XRII the trajectory of the source and detector system must be characterized. High accuracy is needed since errors in calibration propagate through reconstruction process and reduce the accuracy of the result.

We have designed a calibration system using uniquely identifiable markers positioned on a cylinder. This

0-8194-2083-2/96/$6.00

calibration ring is to be placed around the patients head, and consists of steel balls positioned in a predefined arrangement on a cylindrical acrylic support. The balls are arranged such that calibration can be done from almost any partial view, allowing reconstruction of a region of interest (ROI) (see Fig. 1).

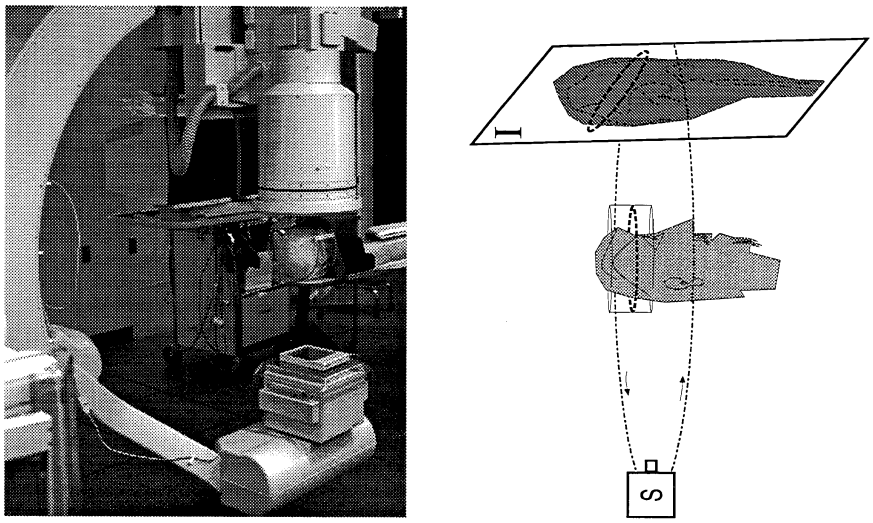

Figure 1: Relative position of X-ray source (S), image intensifier (I), calibration frame and patient's head.

The method has been tested on radiographic data obtained from a single Siemens Neurostar C-arm to determine the optimum design. Steel balls are placed around an acrylic cylinder, restricted to a band approximately 8.5 mm wide, thereby obscuring only a small fraction of the image. In this case the radiograph includes the region of interest (ROI) as well as a partial view of the calibration ring (see Fig. 2). This enables us to recover the geometry of the X-ray imaging system from each individual frame. We call this process "dynamic calibration" as opposed to "off-line" calibration procedures which try to characterize the motion of C-arm before introducing the patient.

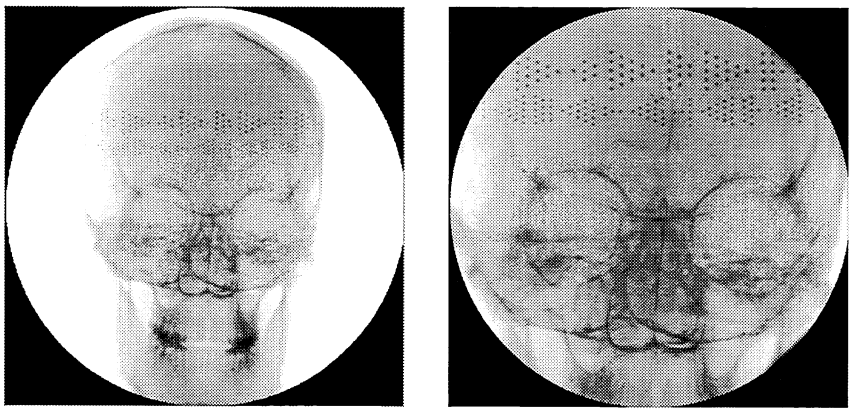

Figure 2: The radiograph includes the region of interest (ROI) as well as a partial view of the calibration ring.

For the calibration scheme proposed here, steel balls are first detected and extracted from each radiograph. 3-D/2-D correspondence between the model of the calibration frame and its image is then established. Finally,

the trajectory of the source and detector system is computed. This last step is similar to what is called "recovery of absolute orientation" in photogrammetry, or "pose determination" in computer vision.

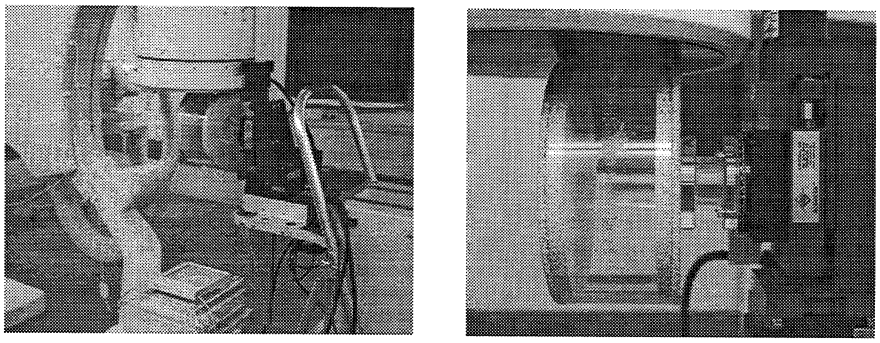

Figure 3: In order to establish the ground truth, our calibration ring is installed on a motion platform which can perform displacements quite accurately.

Experimental validation of the calibration scheme was performed using a prototype version of the calibration ring. The ring was mounted on the rotation axis of a numerically controlled stepper motor (see Fig. 3), and displaced by precisely known amounts (rotational and translational) during image acquisition. Our calibration algorithm was then applied to the sequence of images to recover the inter-frame displacement.

2 DESIGN AND REALIZATION

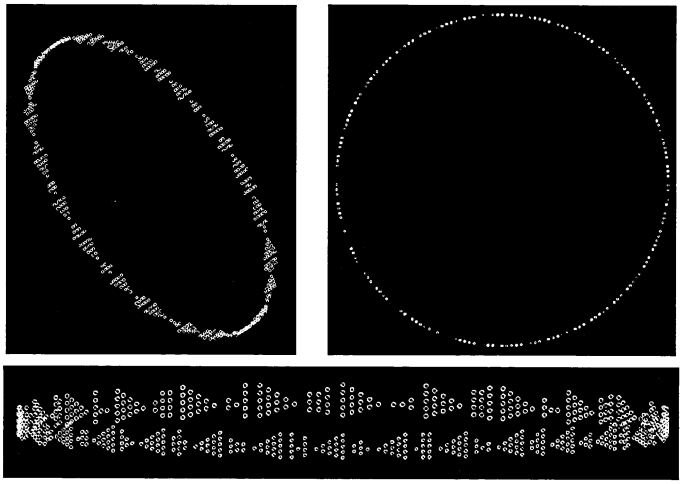

Figure 4: Calibration Ring: a perspective view(left), top view(right), and a typical view in our application(bottom).

The calibration system is composed of a set of landmarks positioned around the patient's head. We call this set of landmarks the "calibration ring". Figure 1 shows the relative position of X-ray source (S), image intensifier (I), calibration ring and patient's head.

A reference coordinate frame is attached to the calibration frame. The three dimensional shape of the calibration frame is precisely known in this coordinate frame. The Steel Balls(SBs) on the calibration frame have a

much higher absorption coefficient than human bones and tissues. This makes the detection/segmentation in the image much easier.

In this design, SBs are arranged vertically around the circumference of the ring. Sequences of such arrangements define code words encoding different sections of the ring.

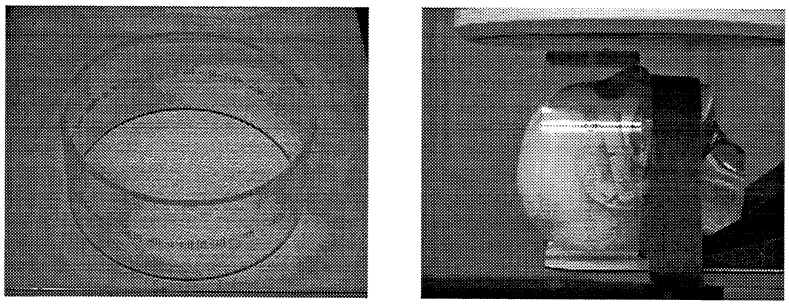

Figure 5: First realization of the Ring for Dynamic Geometrical Calibration for 3-D Cerebral Angiography.

Relative spacing between SBs will vary under perspective projection. Therefore spacing between SBs is not used for encoding the calibration frame. Different spacing is only used in order to facilitate the process of detection and extraction (see section 3). Size of SBs also varies under perspective projection. Difference in size has therefore not been used for encoding purposes. Figure 4 shows the coding on our calibration frame from a top view, a perspective view, and a typical view in our application.

Figure 5 shows a realization of this design*. The radius of the acrylic support cylinder is 112 mm, allowing it to be placed around the head. Steel balls, of diameter $1.2mm$, are placed at 613 positions around the cylinder.

3 DETECTION AND EXTRACTION

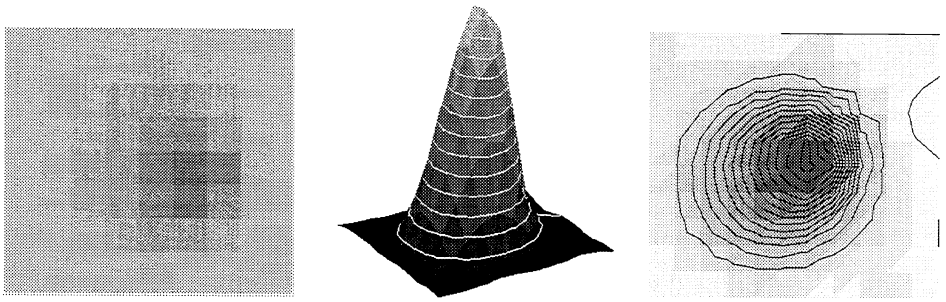

Figure 6: Visualization of the grey value distribution and iso-grey-value curves in radiographic image of steel balls.

The first step of our X-ray Geometrical Calibration system consists of detection and extraction of the SBs from X-ray images. The steel balls on the calibration ring have much higher absorption coefficient than human bones and tissues. They appear therefore as small dark circular areas in the image. Figure 6 shows examples of the distribution of grey level values within the image of a steel ball. Note that this distribution is not always symmetric, due to XRII aberrations. Figure 7 shows the result of Gaussian filtering followed by morphological closing operation on the image of Fig. 6. Only after these operations, thresholding followed by local computation

*This realization was done at University of Western Ontario thanks to Tara Whalen, and Hristo Nikolov.

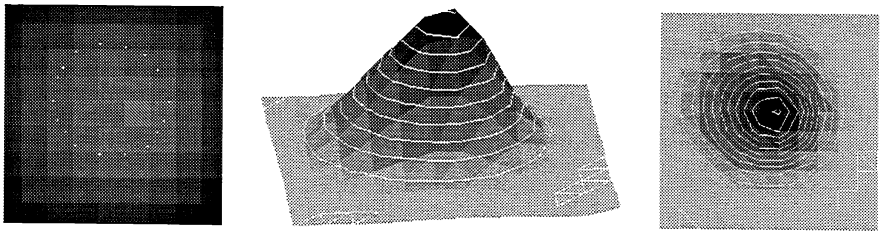

Figure 7: Visualization of the grey value distribution and iso-grey-value curves in radiographic image of steel balls after Gaussian filtering and morphological closing. Results of sub-pixel Canny edge detector on this image is superimposed (white pixels) on the left image.

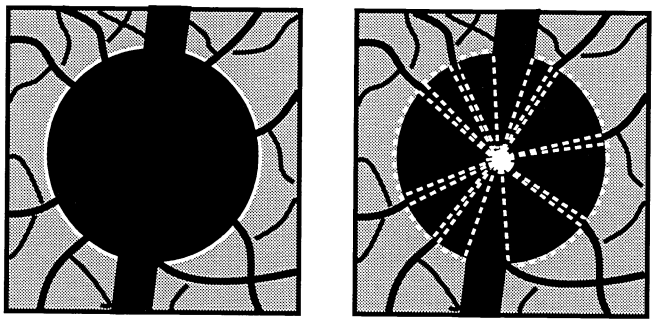

Figure 8: Blood vessels interfere with images of steel balls. Therefore, the contours are often not perfect circles which are easy to extract. Different disconnected segments of circles may be extracted using edge pixel information. They can then be clustered into circles based on their center and radius.

of first moment may result in correct detection and extraction of steel balls. Similar results can be obtained by fitting a circle to edge pixels on the contour of each steel ball. In Fig. 7(left) a sub-pixel Canny edge detector[1] has been applied to the image of a steel ball. This method is more suitable for our application.

In dynamic calibration the ring is placed around the patient's head and the underlying anatomy can interfere with the images of the SBs (see Fig. 8-left). Complete circles are therefore not easy to extract. Different disconnected segments of a circle may be extracted using edge information, and curved segments belonging to the same circles can then be clustered (see Fig. 8-right). A circle fitting algorithm estimates the center and radius of each cluster. Circle detection has therefore been decomposed into three consecutive steps: a) detection of all intensity edges in the image or in an area of interest, b) extraction of edge pixel chains which could belong to the contour of a steel ball, c) clustering of the edge pixel chains obtained in (b) in order to extract the center and radius of the SBs. As well as locating edge pixels, the Canny edge detector measures the intensity gradient $\mathbf{g} = [g_x, g_y]$. The gradient provides sharpness and orientation of an edge at each pixel $[x, y]$. This information can be used to define covariance matrices associated with each edge pixel. The main idea is that sharper edges are more accurately located, and an edge pixel is precisely located in the direction of the gradient of intensity, and not in the tangential direction. This information can be used for weighting the contribution of each detected circle.

4 DECODING AND 3-D/2-D MATCHING

Once images of steel balls are detected in a radiograph, 3-D/2-D correspondences between SBs on the Ring and their radiographic image has to be established. This is done by first separating the upper and lower coded

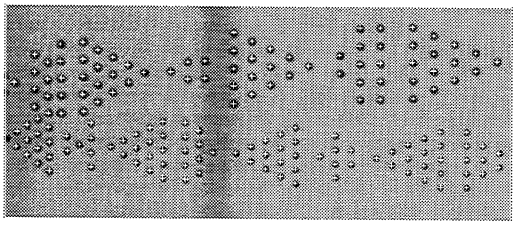

(a) Radiograph of a part of the Calibration Ring.

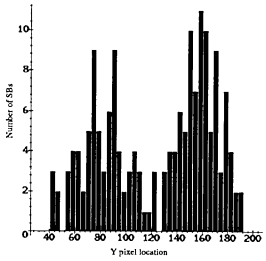

(b) Vertical distribution of circles.

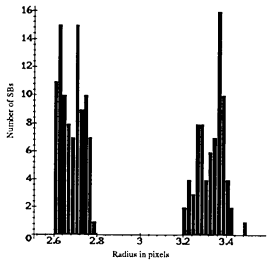

(c) Radius of detected circles.

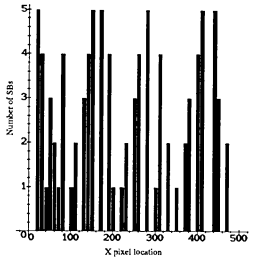

(d) Distribution of circles in lower band.

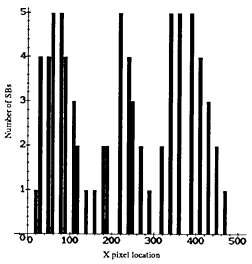

(e) Distribution of circles in upper band.

Figure 9: a) The perspective projection of front part and rear part of the ring onto image plane form two distinguishable bands. Separation of the upper and lower coded bands is done by studying two histograms: b) size of circles, and c) their vertical distribution. In each band, (d) and (e), decoding is done by counting number of circles in columns of 3 pixel wide.

bands. In general, the center of the ROI is near the image center, and the ring is located in the upper or lower part of the image. The plane of the ring is therefore not on the optical axis. The perspective projection of the front and rear parts of the ring onto the image plane form two distinguishable bands (see Fig. 9-a). Images of SBs located in the front part of the ring appear larger than the others. Separation of the upper and lower coded bands is done by studying two histograms. The first histogram is the vertical distribution of circles, i.e the location of centers (see Fig. 9-c). The other histogram is that of the size of circles (see Fig. 9-b).

In each band decoding is done by counting the number of circles in columns of width 3 pixels (see Fig. 9-d and Fig. 9-e). This results in a sequence of numbers for each of the upper and lower bands. These sequences are compared with our original code on the calibration ring. We find a set of reliable code words and match them against our 3-D model. This is the first step to our matching process, resulting in an initial set of correspondences. An initial estimation of the projection matrix can then be obtained (see section 5 for more details). The 3-D model of the calibration ring is then projected onto the image and more correspondences are made by matching each projection with its nearest circle, within a small neighborhood in the image. This step increases the number of correspondences dramatically. Note that in the first step a code word with a missing element is disregarded since

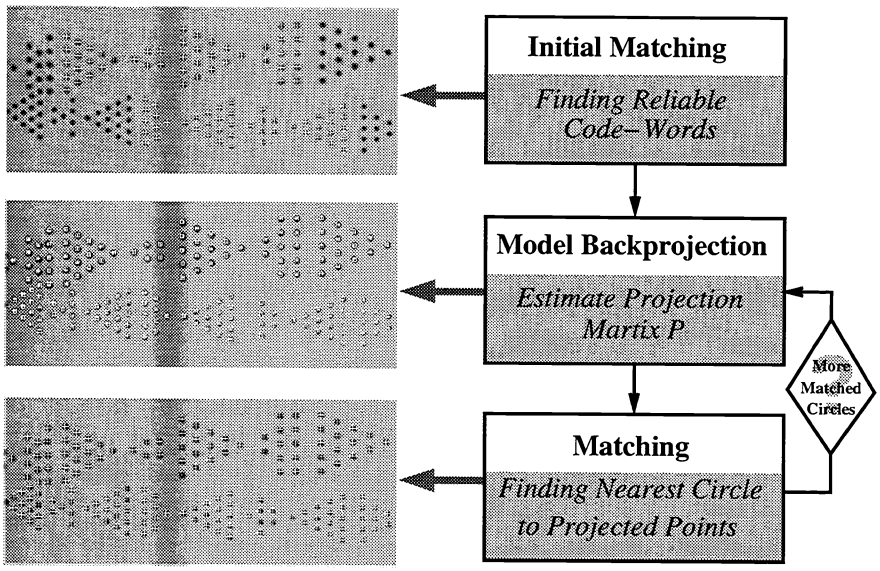

Figure 10: Different steps of the Matching process with examples in a region of interest.

it has no match. If enough circles are matched in the first step, then in the second step almost all visible circles find their correspondences through a back-projection/matching process. By repeating this process the number of correspondences increases. Figure 10 shows the diagram of the matching process along with an example on a radiographic image of the ring.

5 GEOMETRICAL CALIBRATION

The process of computing the trajectory of the source and detector system from a set of 3-D/2-D correspondence is similar to what is called "recovery of absolute orientation" in photogrammetry, or "pose determination" in computer vision. However, the existing techniques do not give satisfactory results because the imaging conditions and the expected accuracy are different. In photogrammetry very often the cameras are far from the scene and long lens cameras are used for photography. The effect of perspective is less important in those cases. In the C-arm geometry the object is between the X-ray source and the image plane, therefore the perspective effect is much higher.

In medical imaging literature Rougée et al.[6] have recently proposed a geometrical calibration method for 3-D X-ray imaging. Based on results reported by Rougée et al.[5] and Faugeras[2] we decided to use a linear method to solve for geometrical calibration. Rougée et al.[6] report that if a large number of points (26 bullets) are used for calibration the accuracy of using a linear method is similar to that of using a non-linear one. Faugeras[2] shows that non-linear methods are advantageous only when inaccuracy in detection is higher than some threshold. In our case an average of 200 to 300 steel balls are used for calibration, and accuracy in detection is high enough to justify the use of a linear system. We have therefore used a linear formulation of the problem.

In the linear approach a 3x4 projective matrix is first computed. If $\mathbf{M}$ is a 3-D point and $\mathbf{m}$ its image, there exists a projection matrix $\mathbf{P}$ such that:

$$\mathbf{m} \cong \mathbf{PM}$$

The projection matrix $\mathbf{P}$ can be written as $\mathbf{P} = \mathbf{A}\ [\mathbf{R}\ \mathbf{T}]$ where the 3×3 rotation matrix $\mathbf{R}$ and the 3-D vector $\mathbf{T}$ define the orientation and location of the camera in the world coordinate system. The upper triangular matrix $\mathbf{A}$, called the matrix of intrinsic parameters, characterizes our imaging system independent of its spatial location and orientation. If images are corrected for radial distortion in our camera model, matrix $\mathbf{A}$ is a function of focal

length, image center, and horizontal and vertical aspect ratios.

Matrix $\mathbf{P}$ can be computed using a weighted least square method or other methods such as the one proposed by Faugeras and Toscani.[3] Different approaches have been taken to decompose the matrix $\mathbf{P}$ into extrinsic, $(\mathbf{R}, \mathbf{T})$, and intrinsic parameters, $\mathbf{A}$.[4,2] These methods mostly take into consideration the fact that $\mathbf{R}$ is an orthonormal matrix satisfying the constraint $\mathbf{R}^t\mathbf{R} = \mathbf{I}$, where $\mathbf{I}$ is the 3×3 identity matrix. $\mathbf{P}$ can be written as $[\mathbf{P}_{13}\mathbf{P}_4]$ where $\mathbf{P}_{13} = \mathbf{AR}$ and $\mathbf{P}_4 = \mathbf{AT}$. We have therefore:

$$\mathbf{P}_{13}\mathbf{P}_{13}^t = \mathbf{ARR}^t\mathbf{A}^t = \mathbf{AA}^t$$

The upper triangular matrix $\mathbf{A}$ can then be computed, followed by computation of $\mathbf{R}$ and $\mathbf{T}$ (see ref.2 for more details). There are now two possibilities for characterizing the geometry of a moving camera. We call these two approaches 1) Pose + Pose, and 2) Pose + Inter-motion. In the first approach extrinsic $(\mathbf{R}_i, \mathbf{T}_i)$, and intrinsic parameters $\mathbf{A}_i$ are obtained for each position of the camera during its motion. The camera motion between two frames i and j is then computed as $\mathbf{R}_{ij} = \mathbf{R}_j\mathbf{R}_i^t$ and $\mathbf{T}_{ij} = -\mathbf{R}_{ij}\mathbf{T}_i + \mathbf{T}_j$. The second approach consists of computing the inter-motion directly from projection matrices $\mathbf{P}_i$ and $\mathbf{P}_j$, supposing that between two consecutive frames intrinsic parameters stay the same:

$$\tilde{\mathbf{R}}_{ij} = k\mathbf{P}_{j13}^{-1}\mathbf{P}_{i13} \quad \text{and} \quad \mathbf{T}_{ij} = \mathbf{P}_{j13}^{-1}(k\mathbf{P}_{i4} - \mathbf{P}_{j4})$$

$\tilde{\mathbf{R}}_{ij}$ computed in this way is not always a Rotation matrix. The orthogonality constraint is then used to improve the results and obtain a real rotation matrix $\mathbf{R}_{ij}$. Through a set of exhaustive tests on synthetic as well as real data we came to the conclusion that this approach results in much more accurate estimations of $\mathbf{R}_{ij}$ and $\mathbf{T}_{ij}$.

6 RESULTS

Validation of our calibration scheme must be done against a ground truth. The ground truth in this case consists of the accurate determination of the geometry of a rotating C-arm relative to a static calibration phantom. This ground truth is difficult to obtain. Another way of establishing the ground truth is to keep the C-arm static and move the calibration ring. This procedure results in similar radiographs. The calibration ring was therefore installed on a motion platform which can perform displacements (combination of rotation and translation) quite accurately (see Fig. 3). The ground truth was then established by applying given rotations and translations to the motion platform and taking a sequence of radiographs. Our calibration algorithm was then applied to these sequences in order to recover the inter-frame displacements. The experiments were conducted at both the University of Western Ontario(UWO), and the Siemens Medical in Erlangen. The motion platform in both cases has three degrees of freedom. It can translate in two orthogonal directions. One axis of motion is parallel (as much as it can be manually positioned) to the image plane along the horizontal direction. The other one is orthogonal to the image plane (toward the X-ray source). Let us call these axes x and y respectively. The ring also rotates around the z axis which is almost parallel to the image plane.

In UWO, two images were taken after pure translations of $10mm$, one parallel to the image plane, and the other one towards the image plane. Then, a sequence of nine consecutive rotations of 5 degrees (about the z-axis) were applied to the ring. This resulted in 11 images, two with pure translations, and 9 with pure rotations. To check the accuracy, we computed; (i) the angle of rotation, (ii) the vector of translation, and (iii) the rotation axis; and compared these with the ground truth measured by the motion platform. It is important to note that accurate computation of the axis of rotation is essential for accurate computation of the angle of rotation and the norm of translation. The ground truth shows translations of:

$$\mathbf{T}_1 = [0.0, 10., 0.0], \qquad \mathbf{T}_2 = [-10.0, 0.0, 0]$$

The estimated translations are:

$$\tilde{\mathbf{T}}_1 = [.007, 10.514, -0.04], \qquad \tilde{\mathbf{T}}_2 = [-9.974, -.688, -0.01]$$

$\mathbf{T}_1$ represents a motion toward the camera (along y-axis) and therefore it is similar to a small change in focal length or a small zooming effect. This explains why we get an error up to $.7mm$ in this direction. Fortunately 3-D

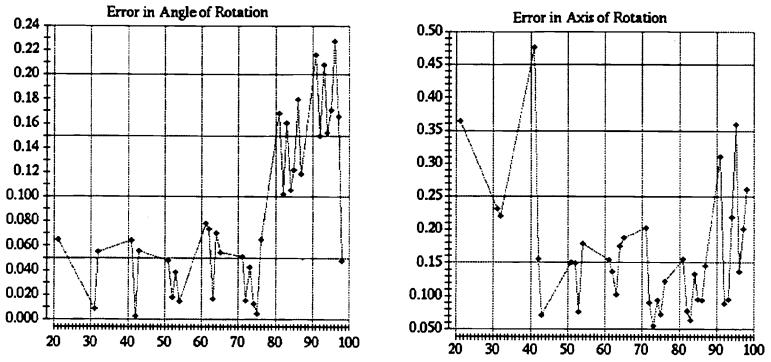

Figure 11: Errors in computation of angle and axis of rotation. The two digit numbers nm (n and m) on the horizontal axis represent the image numbers n and m. The vertical axis represents the errors in the estimation of angle of rotation (left) and in the estimation of orientation of axis of rotation (right) in *degrees*.

reconstruction algorithms are not sensitive to this kind of error. Translational motion parallel to the image plane is estimated quite accurately (less than $0.04mm$). Graphs in Fig. 11 illustrate the estimated errors in computing

T_x	$\tilde{T}_x$	$\tilde{T}_y$	$\tilde{T}_z$
4	4.027	.351	−.013
4	3.967	−.500	.008
8	8.054	.396	−.057
8	7.970	−.506	.005
12	12.023	−.123	−.051
16	16.031	.119	−.057
32	32.025	.113	.086
36	36.051	.468	.093
40	39.981	−.409	.091
48	48.071	−.037	.009

Table 1: Results on the estimation of translational motion in millimeters.

the angular motion and the axis of rotation for our 36 distinct image pairs obtained in our pure rotation sequence. In all graphs, the two digit numbers nm (n and m) on the horizontal axis represent angle difference between the image n and image m. For example, number 38 on the horizontal axis means the angular motion computed between the 3rd and 8th images. The corresponding y-value on the graph, shown by a diamond, is the computed angular error in degrees. The estimated angle between all pairs in the first 7 frames are less than 0.1 degrees. The error involving images 8 and 9 suggests an inaccuracy in the ground truth measurement. Next graph shows the error in the estimated axis of rotation. This is the angle between the estimated axis of rotation and the ground truth (in degrees). At Siemens Medical in Erlangen, the ring phantom was once again fixed to a movable stage. The phantom has been moved parallel to x-axis. Projection images has been acquired every $4mm$. Results are shown in table 6. 11 translational motions parallel to the image plane are reported in this table. The estimated mean error is $0.036mm$ with an standard deviation of 0.016.

The ring has then been rotated from 0 to 360 degrees in steps of 15 degrees. This makes a total of 25 images. The 0 degree and 360 degree images should result theoretically in exactly the same projection images. In practice a small deviations has been found. Preliminary results on the estimation of rotational motion are presented in table 6. There have been 24 motions of $15degrees$ rotation around z-axis. The estimated mean angle of rotation is $15.005degrees$, i.e. no systematic bias, with an standard deviation of 0.084.

Frames	*Angle of Rot.*	*Axis of Rotation*			$\|\tilde{trans}\|$
0 - 15	14.999963	0.015267	-0.000971	0.999883	0.0944
15 - 30	15.022962	0.009200	-0.004927	0.999946	0.0612
30 - 45	15.000049	-0.012141	0.005100	0.999913	0.1298
45 - 60	15.046781	-0.005955	0.004811	0.999971	0.0666
60 - 75	15.053401	-0.006362	0.012781	0.999898	0.1552
75 - 90	15.140636	0.004642	-0.023413	0.999715	0.3831
90 - 105	15.113590	-0.000694	0.033034	0.999454	0.8334
105 - 120	14.959623	-0.012296	-0.037059	0.999237	0.3518
120 - 135	14.948721	0.004153	0.008575	0.999955	0.1423
135 - 150	15.121253	0.041208	0.036320	0.998490	1.0520
150 - 165	14.807315	-0.015513	-0.009768	0.999832	0.5692
165 - 180	15.058728	-0.035507	-0.009750	0.999322	0.1155
180 - 195	14.929314	-0.007180	-0.001841	0.999973	0.0927
195 - 210	15.009136	0.007100	-0.002350	0.999972	0.0660
210 - 225	14.980520	0.035557	-0.021981	0.999126	0.3584
225 - 240	15.099404	-0.020352	0.019377	0.999605	0.3017
240 - 255	15.090319	0.014251	-0.021769	0.999661	0.6697
255 - 270	14.984692	-0.009988	0.035579	0.999317	0.3227
270 - 285	14.911965	-0.001855	-0.015444	0.999879	0.6010
285 - 300	14.810846	0.002649	0.013349	0.999907	0.6571
300 - 315	14.963170	0.006554	0.012571	0.999900	0.4732
315 - 330	14.984937	0.006619	0.006056	0.999960	0.2608
330 - 345	15.014656	-0.031782	-0.016380	0.999361	0.0933
345 - 360	15.000405	0.008137	-0.000767	0.999967	0.3299

Table 2: Some results on the estimation of rotational motion of calibration ring and movable platform at Siemens Medical in Erlangen. Anlges of rotation are in degrees. $\|\tilde{trans}\|$ is the norm of residual translation in millimeters.

7 Conclusion

A calibration ring has been designed to be placed around the patient's head during radiographic image acquisition by a C-arm XRII. An algorithm has been proposed to establish correspondences between the 3-D model of the calibration ring and its radiographic images. A mathematical method has been proposed in order to characterize the motion of a clinical C-arm mounted XRII. The procedure has been validated. The rotation angle and the translational motion parallel to the image plane are estimated accurately. The next step in this research is to verify the precision of this process under realistic clinical conditions (in the presence of human anatomy in the image).

8 REFERENCES

[1] J.F. Canny. Finding edges and lines in images. A.I. Memo. 720, MIT. Artif. Intell. Lab, Cambridge, MA, 1983.

[2] O.D. Faugeras. *Three-Dimensional Computer Vision: A Geometric Viewpoint.* MIT Press, Cambridge, MA, 1993.

[3] O.D. Faugeras and G. Toscani. The calibration problem for stereo. In *Proc. IEEE Conf. Comput. Vision Pattern Recog.*, pages 15–20, Miami, FL, June 1986. IEEE.

[4] S. Ganapathy. Decomposition of trnasformation matrices for robot vision. In *Proc. International Conference on Robotics and Automation*, pages 130–139, 1984.

[5] A. Rougée A. C. Picard Y. Trousset and C. Ponchut. Geometrical calibration for x-ray imaging chains for three dimensional reconstruction. In *Satellite symposium on 3D advanced image processing in medicine*, Rennes, France, Nov. 1992. IEEE-EMBS 14th An. Int. Conf.

[6] A. Rougée A. C. Picard Y. Trousset and C. Ponchut. Geometrical calibration for 3d x-ray imaging. In *Image Capture, Formatting, and Display*, volume 1897, pages 161–168. SPIE, February 1993.